Energy & Environmental Science

Cite this: *Energy Environ. Sci.*, 2012, **5**, 8335

www.rsc.org/ees

PAPER

Bifunctional anode catalysts for direct methanol fuel cells

Jan Rossmeisl,*[ab] Peter Ferrin,[a] Georgios A. Tritsaris,[b] Anand Udaykumar Nilekar,[a] Shirlaine Koh,[cf] Sang Eun Bae,[d] Stanko R. Brankovic,[cd] Peter Strasser[e] and Manos Mavrikakis[a]

Received 14th October 2011, Accepted 7th June 2012
DOI: 10.1039/c2ee21455e

Using the binding energy of OH* and CO* on close-packed surfaces as reactivity descriptors, we screen bulk and surface alloy catalysts for methanol electro-oxidation activity. Using these two descriptors, we illustrate that a good methanol electro-oxidation catalyst must have three key properties: (1) the ability to activate methanol, (2) the ability to activate water, and (3) the ability to react off surface intermediates (such as CO* and OH*). Based on this analysis, an alloy catalyst made up of Cu and Pt should have a synergistic effect facilitating the activity towards methanol electro-oxidation. Using these two reactivity descriptors, a surface $PtCu_3$ alloy is proposed to have the best catalytic properties of the Pt–Cu model catalysts tested, similar to those of a Pt–Ru bulk alloy. To validate the model, experiments on a Pt(111) surface modified with different amounts of Cu adatoms are performed. Adding Cu to a Pt(111) surface increases the methanol oxidation current by more than a factor of three, supporting our theoretical predictions for improved electrocatalysts.

Introduction

Direct methanol fuel cells (DMFCs) offer an attractive alternative to PEM hydrogen fuel cells that circumvents the problem of hydrogen storage.[1] However, the overall energy efficiency of DMFCs is much lower than that of their H_2-PEM counterparts. This is mainly because of the high overpotential necessary to oxidize methanol at the anode of DMFCs.[1–3] While methanol electro-oxidation (the anode reaction in DMFCs) has an equilibrium potential similar to that of the hydrogen oxidation reaction (the anode reaction in H_2-PEM fuel cells),[2] the complex reaction mechanism on these catalysts requires an applied overpotential. Related to this problem is the issue of anode electrocatalyst poisoning: CO is a natural intermediate in methanol electro-oxidation (MOR), binding very strongly to precious metal catalysts, such as Pt. Removing strongly bound CO through oxidation requires a relatively high potential. Steps and defects on Pt are known to decrease the potential for CO oxidation and thereby also help the MOR.[4] Surfaces with relatively weak binding of CO (such as the group 11 metals), however, are not generally able to activate methanol sufficiently. Alloy catalysts have been proposed to overcome these technical issues. The well-known PtRu catalyst is effective as an anode material.[5–10] However, both Pt and Ru are expensive, leaving room for development of active but cheaper electrocatalysts.

[a]*Department of Chemical and Biological Engineering, University of Wisconsin-Madison, 1415 Engineering Drive, Madison, WI 53706, USA. E-mail: jross@fysik.dtu.dk*
[b]*Center for Atomic-scale Materials Design, Department of Physics, Technical University of Denmark, Kgs. Lyngby 2800, DK*
[c]*Department of Chemical and Biomolecular Engineering, University of Houston, 4800 Calhoun Rd, Houston, TX 77204-4004, USA*
[d]*Department of Electrical and Computer Engineering, University of Houston, 4800 Calhoun Rd, Houston, TX 77204-4004, USA*
[e]*Department of Chemistry, Chemical Engineering Division, Technical University Berlin, Strasse des 17. Juni 124, 16123 Berlin, Germany*
[f]*School of Chemical and Life Sciences, Singapore Polytechnic, 500 Dover Road, Singapore 139651*

Broader context

The main idea in this work is to apply atomic scale insight to design effective electrocatalysts for energy conversion and verify the findings with experiments. Direct methanol fuel cells have the large advantage that the fuel has a high volumetric energy density compared to hydrogen. However, the anode reaction is very complicated and thus difficult to catalyze efficiently. The challenge is that the catalyst has to be bifunctional in the sense that it can react with both methanol and water. Even the current best catalyst PtRu is not very efficient. In this work electrocatalytic oxidation of methanol is investigated based on density functional theory calculations. We determine the properties a catalyst for this reaction needs, and identify the fundamental reason for bifunctionality. Based on this insight we predict that PtCu surface alloys should be bifunctional. Experiments provide proof of concept, supporting the theoretical approach.

Past years have witnessed a large number of experimental studies focusing on improving the MOR activity of the Pt–Ru system by adding a third or fourth metal to PtRu.[3,11] Combinatorial and high-throughput experimental screening techniques often helped in this process.[12,13] Accordingly, Reddington *et al.*[14] reported an optical parallel screening method for discovering promising alloy electrocatalysts. Their empirical search highlighted novel Pt–Ru–Ir–Os electrocatalysts with improved methanol oxidation characteristics. To overcome the severe pH limitations of optical screening techniques, a screening platform based on individually addressable multi-electrode arrays was developed.[15] The multi-electrode array enabled direct parallel measurement of catalytic activity.[16] Further, theoretical methods and the available computational power have reached a level where quantum mechanical simulations can be used for understanding and directing catalyst design.[17–20] Guided by first principle predictions of the CO tolerance of ternary Pt–Ru–M alloys, Strasser *et al.* discovered an active class of Co-rich Pt–Ru–Co methanol oxidation catalysts.[21,22] The superiority of this system was later confirmed in an independent study by Cooper and McGinn.[23] The density functional theory (DFT) prediction suggested that Co exerts a ligand effect on Pt surface atoms, reducing the CO chemisorption energy. It was concluded that the coverage of strongly adsorbed CO decreases, while the rate of removal of less strongly adsorbed reactive intermediates increases. Other screening studies geared toward new alloy catalysts with improved methanol oxidation activity reported on Pt–Mo[24] and Pt–Rh[25] binary alloys and Pt–Ru–Ni–Zr,[26] Pt–Ru–Mo–W[27] and Pt–Ru–Rh–Ni[28] quaternary alloys.

In previous work,[29,30] we proposed a framework for the evaluation of catalysts for methanol electro-oxidation. We found that one could describe the necessary applied potential (the MOR potential) as a function of two reactivity descriptors: the adsorption free energy of CO* and OH* on the surface. We also found that the binding energy of other methanol electro-oxidation intermediates scales well with the binding energy of these two intermediates.[31] Two sets of linear relationships were established, one for C-bound species and one for O-bound species. Using this analysis, we identified three major requirements of a good methanol electro-oxidation catalyst. These are the ability to: (1) dehydrogenate methanol completely; (2) activate H_2O; and (3) remove CO* and other intermediates, such as OH*, from the surface. Furthermore, we described the inherent Sabatier behavior associated with the MOR potential, wherein intermediate binding of both reactivity descriptors leads to the lowest MOR potential, and thus, potentially the most efficient catalyst. Using this analysis, we also described the mechanism by which the overall reaction could occur on a given catalyst surface.

Given this framework, one can screen alloys as potential catalysts for methanol electro-oxidation. Alloy bifunctionality can be obtained since the binding energies of CO* and OH* are not closely correlated. This means that one can tune bimetallic alloy components more or less individually towards more favorable catalytic reactivity. First, one can identify the inherent limitation to electro-oxidation with the individual alloy components. For example, let us consider the PtRu system. Pt, the best monometallic catalyst for this reaction, can oxidize methanol to CO* but has difficulty activating H_2O. Ru, on the other hand, can activate H_2O readily, but binds OH* so strongly that it makes its removal difficult. Alloying the two metals provides synergy, where both CO* and OH* can be removed more easily. Similarly, C-bound species adsorb on Cu and Sn too weakly, meaning that both have difficulty with activating the dehydrogenation of these intermediates. For CO oxidation with water, Cu is likely to be active since it is the catalyst of choice for the water–gas-shift reaction[32,33] and other related reactions, such as the electro-reduction of CO_2. This analysis suggests that alloys combining the good properties of Pt towards methanol activation together with the good water activation properties of Cu may have desirable methanol electro-oxidation properties.

In this paper we investigate the first-principles based design of bifunctional catalysts for DMFC anodes. We use the binding of CO* and OH* as reactivity descriptors and apply them on Pt–Ru and Pt–Sn to show the synergistic effects of the alloy components in forming a better methanol electro-oxidation catalyst. Additionally, we calculate the binding of CO* and OH* on bulk and surface Pt–Cu alloys, which are found to have desirable properties for the MOR. We then synthesize and characterize Pt–Cu alloys to confirm the synergistic effect predicted from theory for Cu and Pt in connection to methanol electro-oxidation.

Methods

Theoretical methods

The free energy of various adsorbates on each surface is calculated by employing DFT as implemented in DACAPO, a total energy code.[34–36] A periodic 2×4 unit cell (corresponding to 1/8 ML coverage for each adsorbate) with three layers of metal atoms in each slab and at least five equivalent layers of vacuum between successive slabs is used throughout this study. Metal atoms are kept fixed at their optimized bulk positions, as selected calculations showed that surface relaxation has only small effects on the energetics of the systems studied. The fcc(111) facet of Cu and Pt is modeled. For Ru and Sn, the hcp(0001) surface is employed. In this study, all Pt–Cu alloys, Ru_1Pt_3 and Ru_1Pt_1 alloys are modeled as fcc structures, while Ru_3Pt_1 and Sn_3Pt_1 are modeled as hcp. Energy minimization with respect to lattice constant was performed for all metal and metal alloys studied. Surface alloys ($A_{4-x}B_x$/C, with $x = 1$, 2, or 3) are modeled by replacing atoms of the topmost layer of a slab of C atoms with A and B atoms in the ratio indicated by the appropriate surface stoichiometry. Adsorption of all species is allowed on only one of the two exposed surfaces of each slab, with the dipole moment adjusted accordingly.[37,38] Ionic cores are described by ultrasoft pseudopotentials.[39] The Kohn–Sham one-electron states are expanded in a series of plane waves with an energy cutoff of 25 Ry. The surface Brillouin zone is sampled using a $4 \times 2 \times 1$ Monkhorst-Pack grid.[40] The total energy and potential are described self-consistently, using the PW91 exchange-correlation functional.[41] The energetics determined is sufficiently accurate to determine relative reactivities (*i.e.*, trends) for the electro-oxidation of methanol across the transition metal series. We include corrections for change in zero-point energy (ZPE) and entropy as calculated from vibrational frequencies relative to the reference species, as outlined in ref. 29.

All free energies are calculated relative to $H_2O(l)$, $CO_2(g)$, and $H_2(g)$; the free energy of methanol is calculated from the reaction

$$CO_2(g) + 3H_2(g) \rightarrow CH_3OH(g) + H_2O(l),$$

as follows:

$$G_{CH_3OH} = TE_{H_2O} + TE_{CH_3OH} - TE_{CO_2} - 3*TE_{H_2} + ZPE_{H_2O} + ZPE_{CH_3OH} - ZPE_{CO_2} - 3*ZPE_{H_2} - T*(S_{H_2O} + S_{CH_3OH} - S_{CO_2} - 3*S_{H_2}),$$

where TE is the total energy of reactant and product species calculated with DFT, T is the standard temperature (298 K), ZPE is the zero-point energy for the species as calculated from the respective vibrational frequencies, and S is the entropy of the respective species.

Free energies of surface intermediates are also calculated in a similar manner, *e.g.*:

$$CO_2(g) + 2H_2(g) + * \rightarrow CHOH* + H_2O(l)$$

$$G_{CHOH*} = TE_{H_2O} + TE_{CHOH*} - TE_{CO_2} - 2*TE_{H_2} - TE_{clean} + ZPE_{H_2O} + ZPE_{CHOH*} - ZPE_{CO_2} - 2*ZPE_{H_2} - T*(S_{H_2O} + S_{CHOH*} - S_{CO_2} - 2*S_{H_2}),$$

where TE_{clean} is the total energy of the clean slab and the other terms as described above.

To determine potentials required for the oxidation reaction, we apply the computational standard hydrogen electrode (SHE).[42] The MOR potential of the reaction is defined as the minimum bias at which at least one reaction pathway from reactants to products is downhill in free energy. Since the application of the potential bias U lowers the chemical potential of electrons by eU (where e is the charge of an electron), the free energy of any one reaction step forming an electron is described by

$$\Delta G(U) = \Delta G_{SHE} - eU$$

where ΔG_{SHE} is the free energy change for that step at 0 V *versus* the SHE. Since ΔG is a function of potential, there exists a MOR potential (U_{MOR}), defined as the lowest potential at which the overall reaction can take place. This can be mathematically described as

$$U_{MOR} = \min\left(\max\left(\frac{\Delta G^i_{SHE}}{e}\right)\right)_j$$

where i refers to elementary steps along a given pathway and j are all possible pathways from methanol to CO_2. The reaction step that determined this potential is referred to as the potential-determining step (PDS).

Experimental single crystal electrochemistry

Cleaning and pretreatment procedures. Methanol electro-oxidation reaction was studied using a 10 mm diameter Pt(111) single crystal (0.5 mm thickness). The same crystal was used throughout the entire study. The crystal was immersed in piranic acid (2/3 H_2SO_4 and 1/3 H_2O_2 by volume) for 10 min, after which, it was polished with 0.25 μm diamond paste on nylon pad in circular motions for 5 min or until the crystal surface turned hydrophobic. Next, it was sonicated in ethanol and then in 18.2 MΩ deionized (D.I.) water (Millipore Gradient System) consecutively for 10 min each, before being immersed in piranic acid for another 10 min. The crystal was removed from piranic acid, rinsed in D.I. water again and finally flame-annealed[43,44] in a H_2 flame for at least 20 min, making sure that it was glowing white hot constantly. At the end of 20 min, the crystal was transferred into a cooling chamber filled with 96% Ar and 4% H_2 mixture for 1 h.

Electrochemical set-ups. The electrolytes used for surface structure verification, Cu deposition, and MeOH reactivity measurements were 0.1 M H_2SO_4 (99.9999% purity, Alfa Aesar 11000), 1 mM $CuSO_4$ (Puratonic®, 99.999% purity, Alfa Aesar 10701) in 0.1 M H_2SO_4, and a solution of 0.5 M MeOH (99.93% purity, Sigma Aldrich 494437) in 0.1 M H_2SO_4 respectively. Each electrolyte was kept in individual, commercially acquired electrochemical cells from PINE and ChemGlass Scientific. The working electrode was the Pt(111) single crystal cleaned and annealed as above; the counter electrodes were Pt gauzes. The reference electrode used in connection with the pure H_2SO_4 and MeOH/H_2SO_4 electrolytes was a Ag/AgCl electrode, while a Cu/$CuSO_4$ pseudo reference electrode was used in the $CuSO_4$/H_2SO_4 electrolyte. All reported potentials are with respect to the AgCl scale.

The electrochemical cells were placed inside a glove box together with a beaker of D.I. water to be used for rinsing the Pt(111) single crystal in between characterization, deposition of Cu and reactivity measurements. All electrolytes were de-aerated with N_2 gas prior to the experiment. Once the crystal was cooled to room temperature, it was transferred from the cooling chamber to the glove box and sealed. The air in the glove box was replaced with Ar gas by alternatively pumping down the pressure to ~0.7 atm for 5 min and filling with Ar gas for 10 min for a total of 1.5 h.

Electrochemical Cu deposition and methanol electro-oxidation activity measurements. To check the state of the crystal, cyclic voltammetry (CV) was performed in N_2 saturated H_2SO_4 electrolyte. The crystal was pretreated with 120 potential cycles between −0.23 V and 0.6 V at a scan rate of 250 mV s^{-1} in order to obtain the steady state outlook of CV for Pt(111) in H_2SO_4, with the prominent bi-sulfate peaks. The Pt based electrochemical surface area (Pt-ECSA) of the crystal was determined using the mean integral charge of the hydrogen adsorption and desorption areas with double-layer current corrected for and using 240 μC cm^{-2}Pt, assuming one H atom is adsorbed to each Pt surface atom.

Next, the single crystal was transferred to the de-aerated $CuSO_4$ and H_2SO_4 solution. The Cu UPD profile of the crystal was first measured by cycling the crystal between potentials of 0.2 V and 0.45 V at 5 mV s^{-1}. In order to estimate the Cu UPD stripping charge of a full Cu monolayer, Cu was deposited at a constant potential at 0.2 V for 30 s before the potential was stepped to 0.5 V for 5 s where Cu stripping occurred. The Cu stripping peak, being very sharp and well suited for integration, was used to obtain the total Cu monolayer UPD stripping charge. Following that, various potentials between 0.2 V and 0.5 V were selected and applied for 30 s before stepping to 0.5 V for 5 s and integration for 5 s. The fractional value between the latter Cu stripping charge and that of the former total Cu UPD stripping charge was used as an estimate for the fractional coverage of the Cu UPD monolayer on the Pt(111) single crystal surface.

The Cu-modified Pt(111) crystal was removed from the electrolyte and inserted into the beaker of de-aerated D.I. water to rinse off any residual Cu^{2+} ions on the crystal surface. Thereafter, the crystal was immersed into the $MeOH/H_2SO_4$ solution and 5 CV potential cycling between the potentials of −0.2 V and 0.5 V were obtained at 50 mV s^{-1} to study the MeOH oxidation reactivity as a function of Cu coverage and potential. Methanol oxidation current densities of pure Pt(111) and Cu-modified Pt(111) were compared at 0.35 and 0.3 V.

Results

Bulk Pt-alloys

Our earlier work on the MOR clearly suggests that the free energies of CO and OH bound to the surface, G_{CO} and G_{OH}, are good descriptors for the MOR potential.[29,30] We have shown that maximizing the activity of the anode reaction on the surface is a tradeoff between its ability to activate water and methanol-based intermediates while simultaneously not binding them too strongly, which would lead to a surface poisoned by CO* or OH*. We also identified the region in the phase space of G_{CO*} and G_{OH*} that minimizes the MOR potential. It is important to note that this is possible because G_{CO*} and G_{OH*} do not scale with each other. This is shown in Fig. 1, where the data points for all the metals and alloys do not fall on a single straight line, as expected in case of a linear scaling. Thus there are more opportunities for independent optimization of the catalyst's reactivity.

The electro-oxidation of methanol to CO_2 proceeds without passing through a CO* intermediate (the direct mechanism), especially at low potentials.[29,45–47] However, due to the strong binding of CO* on the surface, which blocks the active sites for this reaction, this mechanism will likely produce only low currents. Thus, we restrict our analysis to electro-oxidation pathways that go through CO* (the indirect mechanism). Under potentials relevant to this mechanism, the oxidation of surface CO* is favorable, allowing for the cleaning of the surface by complete CO* oxidation. Furthermore, because of the bifunctionality inherent in an alloy catalyst we restrict the reaction path for methanol dehydrogenation to CO* to proceed *via* the reaction path found for Pt. This pathway involves first the loss of all carbonic hydrogen to form COH*, and then further dehydrogenation to CO*. Fig. 1 illustrates the tradeoffs that must be considered along this pathway. Too strong CO* and OH* binding will generate difficulties with removing these species from the surface. Too weak CO* binding translates into difficulty with activating methanol. Catalysts with weak OH* binding will have difficulty with activating water (either to form COOH* or OH*).

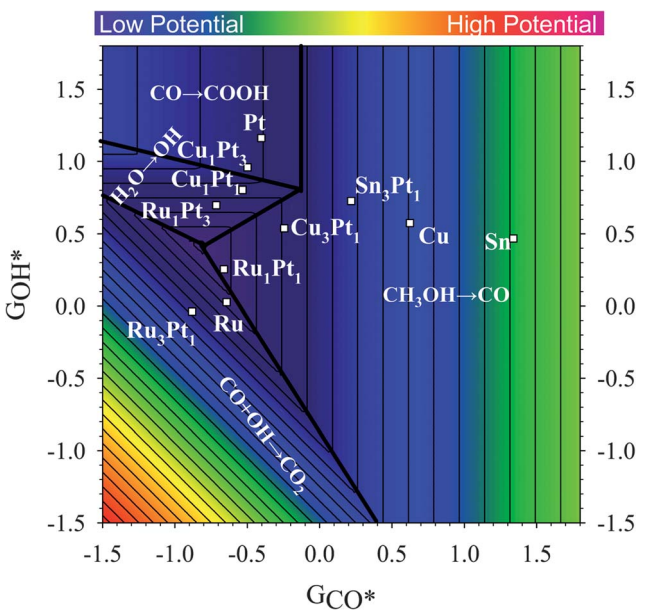

Fig. 1 The volcano plot for the MOR potential of the indirect mechanism with methanol decomposition taking place along the pathway found for Pt(111), using G_{CO*} and G_{OH*} (in eV) as reactivity descriptors. The potential-determining step of each region (outlined in black) is shown. Iso-potential lines are included for reference. Each line represents a difference in MOR potential of 0.1 V. Squares indicate where in the descriptors' phase space the different bulk Pt alloys and pure metals are located. Note that G_{CO*} and G_{OH*} do not scale linearly with each other.

It should be noted that since no reaction rate prefactors were taken into consideration for the construction of the volcano plot in Fig. 1, low MOR potential does not necessarily correspond to high catalytic activity. Comparisons between the activities of any two surfaces can be done only for surfaces lying on the same PDS region of the volcano. We have performed calculations to find the relevant reactivity descriptors for seven different bulk alloys of Pt: $Cu_{4-x}Pt_x$, $Ru_{4-x}Pt_x$ (x = 1, 2, and 3) and Sn_1Pt_3. The respective reactivity descriptor pairs for these alloys and their constituent pure metals are shown in Fig. 1. Examining their relative position on the volcano plot shows that Ru_1Pt_1 and Ru_1Pt_3 are excellent choices for methanol electro-oxidation, which is in good agreement with the experimental literature. Interestingly, Cu_3Pt_1 also proves to be a new promising candidate. Sn_3Pt_1 also has a synergistic effect, as compared with pure Sn. We note that this analysis does not include the effect of solvent. Water will form hydrogen bonds to OH-containing species, with an effect as large as 0.3 eV.[48] This would have the effect of moving the region of CO/OH* poisoning and activation of H_2O up (since OH* would be stabilized). The area of lowest MOR potential would then move towards the Cu_3Pt_1 alloy.

We note in passing that, in general, the binding of an adsorbate on the alloys presented here is an interpolation between the two alloyed pure metals. Generalizing this trend, by using the binding energies for monometallic surfaces, one can easily find alloy stoichiometries that have desirable MOR potentials, using merely the binding characteristics of the component elements. This interpolation principle does not hold for some alloys (*e.g.*, Ru_3Pt_1); these anomalies can be attributed to strain effects. For example, Ru binds OH* slightly more strongly in Ru_3Pt_1 (ref. 49) than in pure Ru. The lattice constant of $PtRu_3$ is larger than pure Ru, stretching Ru and therefore making it more reactive.[49]

Given the simplicity of the model we cannot clearly conclude whether Cu_3Pt_1 has an activity comparable with Ru_1Pt_1, which is known to have excellent properties for methanol electro-oxidation. There is also an added uncertainty as the Pt–Cu systems studied are in a different region of the phase space, meaning that direct comparison is even more difficult. A better comparison could be made if we could find a Pt–Cu system situated in the same PDS region as PtRu. Therefore we then investigated the Pt–Cu system in more detail.

Surface alloys of PtCu

The binding of adsorbates on alloys is typically between the constituent metals as a result of several key effects. One effect is the difference in lattice constant of the alloy as compared to the pure metal components. Pt–Cu bulk alloys have properties intermediate between Pt and Cu (see Fig. 1), partially because of stretching/compressing of the alloy lattice, when compared to the pure metals. The alloy has a lattice constant intermediate to the two components; thus Pt is compressed in the Pt–Cu alloys because Cu has a smaller lattice constant than Pt. The effect of compressive strain on transition metal surfaces is to weaken the binding of adsorbates.[49–51] Thus, species bound to Pt in Pt–Cu alloys will be more weakly bound than on pure Pt, even if they are not directly bound to the Cu component (such as in the case of CO* on Cu_3Pt_1).

In addition to strain effects, there is an important ensemble effect on adsorbate binding. Individual Cu atoms on the surface (such as in the Cu_1Pt_3 alloy, for example) bind OH* quite weakly. The site preference for OH* binding on pure Cu is a three-fold hollow site. However, due to geometric considerations, no site with a pure Cu three-fold hollow exists on an ordered alloy with 25% or 50% Cu on the surface. When there is sufficient coverage of Cu on the surface to form such three-fold ensemble sites, the binding of OH* is significantly increased as compared to Pt.

Given the importance of strain and ensemble considerations on adsorbate binding, the use of surface alloys may allow for further 'tuning' of binding properties. Such alloys have been shown to have desirable properties for other electrochemical reactions, especially oxygen reduction.[50–55] In this case, supporting Cu_3Pt_1 on Pt, for example, would subject the surface alloy layer to an expansive strain; thus, Pt and Cu would be more reactive on this surface than the corresponding bulk alloy. The stronger adsorbate binding on such a surface would move the Cu_3Pt_1 point towards the ideal point on the volcano plot. To illustrate this we have calculated the reactivity descriptors for three surface alloys: Cu_2Pt_2 supported on Cu and Pt ("Cu_1Pt_1*/Cu" and "Cu_1Pt_1*/Pt" respectively), and Cu_3Pt on Pt ("Cu_3Pt*/Pt"). The results are shown in Fig. 2, together with the bulk alloys of Pt–Cu and Pt–Ru. Cu_1Pt_1 supported on Cu is not a good candidate for MOR, as it seems to replicate the weak binding of CO on Cu as well as the weak OH binding on Pt. This is not unexpected, as the compressive strain imposed by the Cu host on the alloy will tend to weaken adsorbate-metal bonds. The surface alloys Cu_1Pt_1*/Pt and Cu_3Pt_1*/Pt, however, share desirable properties.

Importantly, the Pt–Cu systems shown here sample multiple regions of the volcano plot corresponding to different PDS, meaning that they sample a large range of relevant free energy for catalysts running at low potentials. Therefore, one may be able to fine-tune the electrocatalytic activity of the Pt–Cu system by varying the stoichiometry of the surface towards optimal performance.

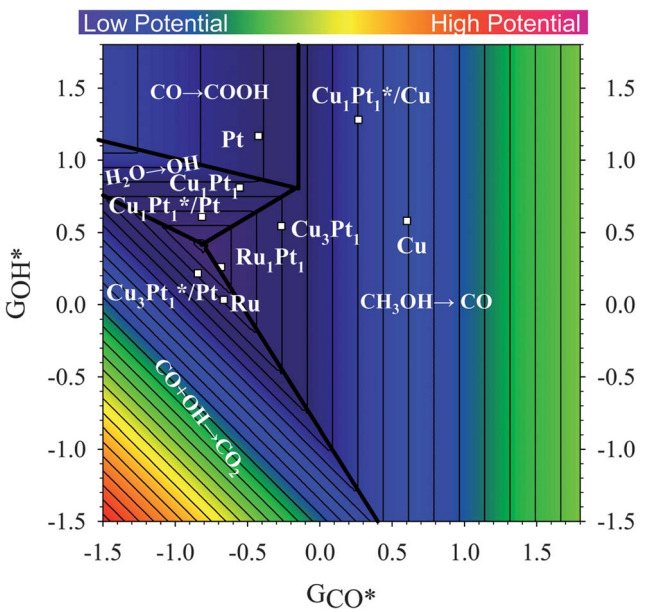

Fig. 2 Positions of selected Pt–Ru and Pt–Cu bulk and surface alloys on the volcano plot for the MOR potential of the indirect mechanism as in Fig. 1. The potential determining step of each region (outlined in black) is shown. Iso-potential lines are included for reference. Each line represents a difference in MOR potential of 0.1 V.

Experimental results

To test our theoretical predictions of the reactivity of Pt and Cu atoms in a Cu_1Pt_1 alloy surface for the electro-oxidation of methanol, we deposited controlled amounts of Cu adatoms on a Pt(111) single crystal surface and performed sweep voltammetry measurements of the electro-oxidation of methanol in acidic solutions.

Fig. 3A shows the cyclic voltammogram of the cleaned Pt(111) single crystal electrode in 0.1 M H_2SO_4, sweep rate 25 mV s^{-1}. The profile shows the familiar broad hydrogen adsorption/desorption region (−0.2 V to 0.07 V), the symmetric sharp sulfate adsorption/desorption features as well as the small Pt–OH formation (anodic scan at 0.45 V) and reduction (cathodic scan at 0.4 V) features. The overall profile represents the classical 'butterfly' feature first described by Clavilier *et al.* in 1980 (ref. 43) representative of a well-defined single crystal surface.[45,56] Controlled amounts of Cu adatoms were then deposited onto the surface of the Pt(111) single crystal electrode by potentiostatic electrodeposition of Cu from a 1 mM $CuSO_4$ solution. Fig. 3B shows the Cu deposition isotherm (open circles) relating the deposition potential to the relative Cu coverage. Around 0.4 V, a dramatic and rapid change in Cu coverage can be observed. The solid cyclic voltammogram depicts a typical Cu upd voltammetric adsorption/desorption profile in the Cu containing solution. This suggests that the Cu-adatom stripping during the anodic scan is completed at around 0.45 V in Cu^{2+} ion containing electrolyte.

We assessed the methanol electrocatalytic activity of the Pt/Cu surfaces using linear sweep voltammetry; cathodic traces at seven different Cu coverage are shown in Fig. 3C. The high-coverage Cu surface and the pure Pt surface show low catalytic peak activities for methanol oxidation relative to those surfaces with intermediate Cu coverage.

In order to evaluate intrinsic synergistic catalytic enhancement effects due to the combined presence of Cu and Pt surface atoms, we have normalized the experimental methanol oxidation current density at two relevant electrode potentials, 0.3 V and 0.35 V, and plotted the obtained normalized catalytic enhancement factor at the two potentials as a function of Cu coverage in

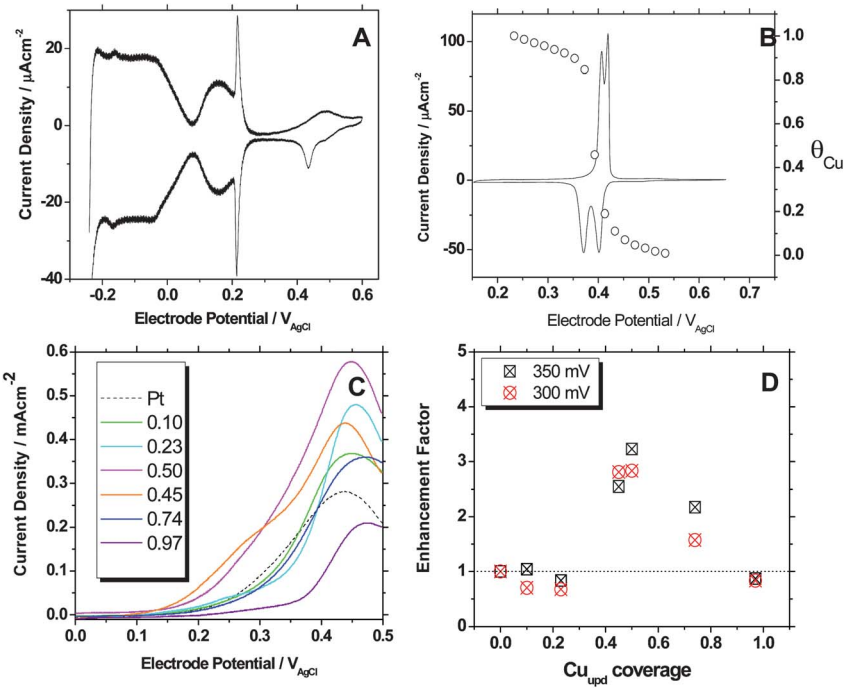

Fig. 3 (A) Cyclic voltammetric profile of the Pt(111) single crystal prior to surface modifications with Cu adatoms. Conditions: 25 mV s^{-1}, de-aerated 0.1 M H_2SO_4. (B) Circles: Cu coverage as function of Cu deposition potential. Cu coverage was determined by stripping at 0.5 V for 5 s. Solid line: cyclic voltammogram, 5 mV s^{-1}, of Cu stripping and Cu deposition. Conditions: 1 mM $CuSO_4$ in 0.1 m H_2SO_4. (C) Methanol oxidation voltammetry of selected Cu/Pt(111) surfaces in comparison to the pure Pt(111) surface. Cu coverage (in ML) is provided in the legend. Conditions: 50 mV s^{-1}, 0.5 M methanol/0.1 M H_2SO_4. (D) Activity enhancement factors of methanol electrooxidation activities at 0.3 V/AgCl and 0.35 V/AgCl as a function of Cu coverage. See text for details of normalization.

Fig. 3D. The normalization current density, j_{norm}, and a catalytic enhancement factor were obtained from

$$j_{norm}(E,\theta) = \theta \times j_{Cu}(E) + (1 - \theta) \times j_{Pt}(E),$$

and

$$\text{Enhancement factor } (E,\theta) = \frac{j(E,\theta)}{j_{norm}(E,\theta)}$$

where θ and E denote the fractional Cu(upd) coverage and the electrode potential, respectively. The normalization current density, j_{norm}, represents the expected combined θ-weighted catalytic methanol oxidation current at any given Cu coverage in absence of any synergistic kinetic effects (mean field approximation). The enhancement factor reveals the experimental excess catalytic activity beyond the combined current densities from Pt and Cu surface atoms alone. The coverage dependence of the enhancement factor in Fig. 3D evidences a significant synergistic kinetic effect on the bimetallic Cu(upd)/Pt(111) surface exhibiting a catalytic enhancement of almost 3.5 fold at Cu coverage of about 0.5 ML and at electrode potentials directly relevant to direct methanol fuel cells. Kinetic enhancements cease at zero and full coverage indicated by an enhancement factor of unity. Interestingly, limited Cu(upd) coverage below 0.3 ML had a detrimental effect on the catalytic activity (enhancement factor below unity) indicating that additional effects, possibly related to anion co-adsorption of sulfate anions, affected the methanol oxidation reaction. The complex interplay between sulfate anion adsorption and underpotentially deposited Cu and their combined effect on the electrooxidation of methanol on Pt single crystals was thoroughly addressed by Markovic and Ross.[57] First, the authors concluded that anion adsorption rather than surface oxide formation is responsible for the methanol electrooxidation current maxima in the 0.4–0.5 V/AgCl range (see Fig. 3C). This effect was more pronounced on Pt(111) than on Pt(100). Also, the authors studied the impact of underpotentially deposited Cu atoms on the methanol oxidation currents. The presence of Cu(upd) surface atoms at a 5% coverage dramatically reduced the methanol oxidation activity by a factor of up to two in a perchloric acid electrolyte or a sulfuric acid environment. Based on these results, we conclude that a coupling of sulfate adsorption and Cu(upd) atoms may be responsible for the slight detrimental effects of Cu(upd) at low coverage, however, this fails to account for the significantly enhanced catalytic activity at higher Cu coverage.

The discrepancy between the optimal Pt–Cu alloy ratio determined from experiments and that predicted by theory (Cu_1Pt_1*/Pt in experiments *vs.* Cu_3Pt_1*/Pt according to the model) may be due to the formation of Cu trimer islands, rather than a true surface alloy; thus the bifunctionality would be occurring along the border of these Cu islands. Preparation of a stable surface alloy is difficult to realize, as annealing in vacuum would make Pt atoms segregate to the surface leaving Cu atoms in the second layer. We note that by annealing in an atmosphere of CO a Cu_3Pt_1 surface alloy could form.[58] We speculate that this might be a possible route to prepare the Cu_1Pt_1 anode. However, even in the present experiments, the synergistic effect born by the simultaneous presence of Pt and Cu on the electrode's surface is evident, supporting the overall analysis.

Conclusions

A DMFC anode needs to (1) oxidize methanol to CO*, (2) activate water (3) and not bind OH* and CO* so strongly that CO_2 formation is hindered. These three features are directly related to the catalyst binding of CO* and OH*, with the most efficient catalysts having moderate binding of both CO* and OH*. Pure Pt is capable of oxidizing methanol to CO*; however, it binds CO* very strongly and has difficulty with activating water, and thus removing CO* from the surface.

On the basis of DFT calculations we analyze different bulk and surface Pt alloys for their methanol electro-oxidation properties. Our theoretical analysis framework indeed predicts that the well-known Pt–Ru and Pt–Sn alloys should have good catalytic properties for this reaction. In addition, Pt–Cu alloys are predicted to be promising catalysts. According to our analysis, the most effective Pt–Cu catalysts will have three-atom ensembles of Cu to activate H_2O but also have a relatively stretched lattice. The Pt–Cu alloy system with properties closest to the ideal is predicted to be the surface alloy Cu_3Pt_1/Pt. This system is calculated to have similar properties to Pt–Ru.

To verify this prediction, experiments on a Pt(111) surface modified with different amounts of deposited Cu were performed. Adding Cu to the Pt(111) surface clearly increased methanol electro-oxidation activity at low potentials, with approximately ½ ML of Cu on a Pt surface performing best of the alloys studied. While Cu on Pt particles will likely have stability problems in electrocatalytic environments, the success of our simple model in predicting novel catalytic surfaces suggests that further analysis along the lines illustrated here may be promising in the search for new bifunctional electrocatalysts.

Acknowledgements

The Center for Atomic-scale Materials Design is funded by the Lundbeck Foundation. UW acknowledges funding through the US Department of Energy, Basic Energy Sciences, Division of Chemical Sciences. Computing time was used at the following institutions: EMSL, a national scientific user facility at Pacific Northwest National Laboratory (PNNL); the Center for Nanoscale Materials at Argonne National Laboratory (ANL); the National Center for Computational Sciences at Oak Ridge National Laboratory (ORNL); and the National Energy Research Scientific Computing Center (NERSC). EMSL is sponsored by the Department of Energy's Office of Biological and Environmental Research located at PNNL. CNM, NCCS, and ORNL are supported by the US Department of Energy, Office of Science, under Contract nos. DE-AC02-06CH11357; DE-AC05-00OR22725; and DE-AC02-05CH11231 respectively. SK and PS acknowledge funding through the US Department of Energy, Basic Energy Sciences *via* a subcontract from Stanford Accelerator Laboratory. PS also acknowledges partial support by the Center of Excellence (Exzellenzcluster) in Catalysis UNICAT, funded by the German National Science Foundation (DFG) and managed by the Technical University Berlin. SRB acknowledges support from NSF Career program # 0955922.

References

1 A. Hamnett, *Catal. Today*, 1997, **38**, 445–457.
2 T. D. Jarvi and E. M. Stuve, in *The Science of Electrocatalysis on Bimetallic Surfaces*, ed. J. Lipkowski and P. Ross, Wiley-VCH, Inc., 1998, pp. 75–152.
3 H. Liu, C. Song, L. Zhang, J. Zhang, H. Wang and D. P. Wilkinson, *J. Power Sources*, 2006, **155**, 95–110.
4 S. C. S. Lai, N. P. Lebedeva, T. H. M. Housmans and M. T. M. Koper, *Top. Catal.*, 2007, **46**, 320–333.
5 P. Liu, A. Logadottir and J. K. Nørskov, *Electrochim. Acta*, 2003, **48**, 3731–3742.
6 S. Surampudi, S. R. Narayanan, E. Vamos, H. Frank, G. Halpert, A. LaConti, J. Kosek, G. K. S. Prakash and G. A. Olah, *J. Power Sources*, 1994, **47**, 377–385.
7 Y. J. Ando, K. Sasaki and R. Adzic, *Electrochem. Commun.*, 2009, **11**, 1135–1138.
8 M. T. M. Koper, T. E. Shubina and R. A. van Santen, *J. Phys. Chem. B*, 2002, **106**, 686–692.
9 H. A. Gasteiger, N. Markovic, P. N. Ross and E. J. Cairns, *J. Phys. Chem.*, 1994, **98**, 617–625.
10 H. A. Gasteiger, N. Markovic, P. N. Ross and E. J. Cairns, *J. Phys. Chem.*, 1993, **97**, 12020–12029.
11 S. Wasmus and A. Kuver, *J. Electroanal. Chem.*, 1999, **461**, 14–31.
12 *High-Throughput Screening in Chemical Catalysis – Technologies, Strategies and Applications*, ed. A. Hagemeyer, P. Strasser and A. F. Volpe, Wiley VCH, Weinheim, 2004.
13 E. S. Smotkin and R. R. Diaz-Morales, *Annu. Rev. Mater. Res.*, 2003, **33**, 557.
14 E. Reddington, A. Sapienza, B. Gurau, R. Viswanathan, S. Sarangapani, E. S. Smotkin and T. E. Mallouk, *Science*, 1998, **280**, 1735–1737.
15 P. Strasser, S. Gorer and M. Devenney, in *Direct Methanol Fuel Cells*, ed. S. R. Narayanan, S. Gottesfeld and T. Zawodzinski, The Electrochemical Society, Washington, 2001, vol. 2001–4, pp. 191–208.
16 P. Strasser, S. Gorer, Q. Fan, K. Chondroudis, K. Cendak, D. Giaquinta and M. Devenney, in *High-Throughput Screening in Chemical Catalysis*, ed. A. Hagemeyer, P. Strasser and A. F. Volpe, Wiley VCH, Weinheim, 2004, p. 271.
17 J. K. Nørskov, T. Bligaard, J. Rossmeisl and C. H. Christensen, *Nat. Chem.*, 2009, **1**, 37–46.
18 J. Greeley and M. Mavrikakis, *Nat. Mater.*, 2004, **3**, 810–815.
19 S. Alayoglu, A. U. Nilekar, M. Mavrikakis and B. Eichhorn, *Nat. Mater.*, 2008, **7**, 333–338.
20 A. U. Nilekar, S. Alayoglu, B. Eichhorn and M. Mavrikakis, *J. Am. Chem. Soc.*, 2010, **132**, 7418–7428.
21 P. Strasser, *J. Comb. Chem.*, 2008, **10**, 216–224.
22 P. Strasser, Q. Fan, M. Devenney, W. H. Weinberg, P. Liu and J. K. Nørskov, *J. Phys. Chem. B*, 2003, **107**, 11013–11021.
23 J. S. Cooper and P. J. McGinn, *J. Power Sources*, 2006, **163**, 330–338.
24 D. A. Stevens, J. M. Rouleau, R. E. Mar, A. Bonakdarpour, R. T. Atanasoski, A. K. Schmoeckel, M. K. Debe and J. R. Dahn, *J. Electrochem. Soc.*, 2007, **154**, B566–B576.
25 W. Tokarz, H. Siwek, P. Piela and A. Czerwinski, *Electrochim. Acta*, 2007, **52**, 5565–5573.
26 J. F. Whitacre, T. Valdez and S. R. Narayanan, *J. Electrochem. Soc.*, 2005, **152**, A1780–A1789.
27 W. C. Choi, Y. J. Kim and S. I. Woo, *Catal. Today*, 2002, **74**, 235.
28 K.-W. Park, J.-H. Choi, S.-A. Lee, C. Pak, H. Chang and Y.-E. Sung, *J. Catal.*, 2004, **224**, 236–242.
29 P. Ferrin, A. U. Nilekar, J. Greeley, M. Mavrikakis and J. Rossmeisl, *Surf. Sci.*, 2008, **602**, 3424–3431.
30 P. Ferrin and M. Mavrikakis, *J. Am. Chem. Soc.*, 2009, **131**, 14381–14389.
31 F. Abild-Pedersen, J. Greeley, F. Studt, J. Rossmeisl, T. R. Munter, P. G. Moses, E. Skulason, T. Bligaard and J. K. Nørskov, *Phys. Rev. Lett.*, 2007, **99**, 016105.
32 C. V. Ovesen, B. S. Clausen, B. S. Hammershoi, G. Steffensen, T. Askgaard, I. Chorkendorff, J. K. Nørskov, P. B. Rasmussen, P. Stoltze and P. Taylor, *J. Catal.*, 1996, **158**, 170–180.
33 A. A. Gokhale, J. A. Dumesic and M. Mavrikakis, *J. Am. Chem. Soc.*, 2008, **130**, 1402–1414.
34 J. Greeley and M. Mavrikakis, *J. Am. Chem. Soc.*, 2002, **124**, 7193–7201.
35 B. Hammer, L. B. Hansen and J. K. Nørskov, *Phys. Rev. B: Condens. Matter Mater. Phys.*, 1999, **59**, 7413–7421.
36 J. Greeley, J. K. Norskov and M. Mavrikakis, *Annu. Rev. Phys. Chem.*, 2002, **53**, 319–348.

37 J. Neugebauer and M. Scheffler, *Phys. Rev. B: Condens. Matter Mater. Phys.*, 1992, **46**, 16067–16080.
38 L. Bengtsson, *Phys. Rev. B: Condens. Matter Mater. Phys.*, 1999, **59**, 12301–12304.
39 D. Vanderbilt, *Phys. Rev. B: Condens. Matter Mater. Phys.*, 1990, **41**, 7892–7895.
40 D. J. Chadi and M. L. Cohen, *Phys. Rev. B: Solid State*, 1973, **8**, 5747–5753.
41 J. P. Perdew, J. A. Chevary, S. H. Vosko, K. A. Jackson, M. R. Pederson, D. J. Singh and C. Fiolhais, *Phys. Rev. B: Condens. Matter Mater. Phys.*, 1992, **46**, 6671–6687.
42 J. K. Nørskov, J. Rossmeisl, A. Logadottir, L. Lindqvist, J. R. Kitchin, T. Bligaard and H. Jonsson, *J. Phys. Chem. B*, 2004, **108**, 17886–17892.
43 J. Clavilier, *J. Electroanal. Chem.*, 1980, **107**, 205.
44 J. Clavilier, D. Armand, S. G. Sun and M. Petit, *J. Electroanal. Chem.*, 1986, **205**, 267.
45 D. Cao, G. Q. Lu, A. Wieckowski, S. A. Wasileski and M. Neurock, *J. Phys. Chem. B*, 2005, **109**, 11622–11633.
46 Y. X. Chen, A. Miki, S. Ye, H. Sakai and M. Osawa, *J. Am. Chem. Soc.*, 2003, **125**, 3680–3681.
47 T. Iwasita, *Electrochim. Acta*, 2002, **47**, 3663–3674.
48 J. Rossmeisl, J. K. Norskov, C. D. Taylor, M. J. Janik and M. Neurock, *J. Phys. Chem. B*, 2006, **110**, 21833–21839.
49 M. Mavrikakis, B. Hammer and J. K. Nørskov, *Phys. Rev. Lett.*, 1998, **81**, 2819–2822.
50 P. Strasser, S. Koh, T. Anniyev, J. Greeley, K. More, C. F. Yu, Z. C. Liu, S. Kaya, D. Nordlund, H. Ogasawara, M. F. Toney and A. Nilsson, *Nat. Chem.*, 2010, **2**, 454–460.
51 J. Greeley, I. E. L. Stephens, A. S. Bondarenko, T. P. Johansson, H. A. Hansen, T. F. Jaramillo, J. Rossmeisl, I. Chorkendorff and J. K. Norskov, *Nat. Chem.*, 2009, **1**, 552–556.
52 A. U. Nilekar and M. Mavrikakis, *Surf. Sci.*, 2008, **602**, L89–L94.
53 A. U. Nilekar, Y. Xu, J. L. Zhang, M. B. Vukmirovic, K. Sasaki, R. R. Adzic and M. Mavrikakis, *Top. Catal.*, 2007, **46**, 276–284.
54 J. L. Zhang, M. B. Vukmirovic, K. Sasaki, A. U. Nilekar, M. Mavrikakis and R. R. Adzic, *J. Am. Chem. Soc.*, 2005, **127**, 12480–12481.
55 J. L. Zhang, M. B. Vukmirovic, Y. Xu, M. Mavrikakis and R. R. Adzic, *Angew. Chem., Int. Ed.*, 2005, **44**, 2132–2135.
56 A. Cuesta, L. A. Kibler and D. M. Kolb, *J. Electroanal. Chem.*, 1999, **466**, 165–168.
57 N. Markovic and P. N. Ross, *J. Electroanal. Chem.*, 1992, **330**, 499–520.
58 K. J. Andersson, F. Calle-Vallejo, J. Rossmeisl and L. Chorkendorff, *J. Am. Chem. Soc.*, 2009, **131**, 2404–2407.

